The role of hydrogen in the corrosion-induced reduction of K_R critical fracture toughness and intergranular secondary cracking in a high-strength aluminium alloy

Christiaan Pretorius[1], and *Roelf* Mostert[1]

[1]University of Pretoria, Department of Materials Science and Metallurgical Engineering, Lynnwood Road, Hatfield, Pretoria 0002, South Africa

Abstract. It is shown that short-term exposure of AA2024-T3 material to an exfoliation corrosion (EXCO) solution leads to a reduction of non-plane strain fracture toughness and the formation of secondary surface cracks during plastic straining. The study aims to establish whether the secondary cracking effect and the fracture toughness reduction are due to corrosion-induced hydrogen embrittlement. It is hypothesized that, if hydrogen-embrittlement is the cause of the intergranular secondary cracking (ISC) and fracture toughness degradation, post-exposure heat treatment would restore the mechanical property degradation and reduce the ISC formation through the desorption of diffusible hydrogen. It was found that the solution and ageing heat treatments restored the fracture toughness of the alloy. However, the ISC behaviour persisted. The results are discussed and interpreted in terms of hydrogen embrittlement theory.

1 Introduction

Over the years, it has been shown that aluminium and its alloys may be susceptible to various types of corrosion attack, including exfoliation corrosion during atmospheric exposure [1]. The type of corrosion attack is dependent on the pH of the exposure environment, the alloy content of the material and the cladding material used, inter. alia. Of particular importance in the current investigation is intergranular type corrosion associated with Al-Cu alloys. According to the literature, this type of attack is a result of chemical heterogeneity between constituents and the surrounding matrix [2-5], which forms a micro-galvanic coupling at this location [1,6]. In the case of Al-Cu alloys, intergranular corrosion has typically been ascribed to the segregation and precipitation of copper and copper-containing precipitates/particles at the grain-boundaries, which results in a copper depleted band in the matrix adjacent to the grain boundary [1]. As such, the more noble Cu-rich grain boundaries may act as cathodes [7], and dissolution may occur within the surrounding anodic (Cu depleted) aluminium matrix. However, Lou et.al [8] showed that the intergranular attack persisted even in the absence of chemical heterogeneity, and Zhang et. al. [9] showed a strong proportional correlation between intergranular corrosion and dislocation density within the grains (or grain-boundary stored energy). Nevertheless, slight copper enrichment within the high-

energy grains was still reported, and it was concluded that the non-uniform Cu-distribution – due to the non-uniform dislocation distribution – results in a galvanic coupling between neighbouring grains.

In addition to intergranular corrosive attack, Petroyiannis et. al. [10] showed that corrosion-induced hydrogen embrittlement contributed to the degradation of both the fracture toughness and tensile properties of aluminium alloy 2024-T3. The tests comprised of the accelerated corrosion exposure of the test specimens to an EXCO solution. Regarding the tensile properties, it was found that the degradation of mechanical strength could be restored by mechanical removal of the corroded layer. However, the degradation of tensile ductility could only be restored via post-exposure heat treatments [10]. Pretorius et.al. [11] investigated the effect of short-term (2 hours) EXCO-exposure on the slow strain-rate crack extension resistance (K_R) behaviour of thin (3.1 mm thick) aluminium alloy 2024-T3 sheet. It was reported that little to no visual indication of general or localized corrosion could be observed after the exposure. However, intergranular surface cracks (ISCs) were observed to form in the crack tip plastic zone during slow-strain-rate loading of the K_R specimens [11]. The ISCs were orientated in a direction parallel to the primary crack, and perpendicular to the exposed surfaces. Fractography also revealed intergranular fracture on the primary crack at locations close to the exposed surface, extending to an approximate depth of 115µm from the exposed surface. A degradation of the critical crack extension resistance *K*-value of 11.2% was reported after corrosive exposure [11].

It was proposed by Larignon et al [12] that grain and sub-grain boundaries act as preferred pathways for the diffusion of hydrogen during the corrosion of aluminium alloy 2024. The reported absence of visible corrosion products on the fracture surfaces in the work by Pretorius et.al. may imply that intergranular hydrogen embrittlement played a role in the formation of the intergranular secondary cracks, and in the degradation of the crack extension resistance. The extent of secondary cracking and the reported degradation of the crack extension resistance indicates that this type of attack is concerning from a structural integrity perspective. Therefore, the current investigation replicates the the conditions investigated by Pretorius et.al. [11] to study the degradation in more detail. Additional tests are performed on AA2024-T3 subjected to a post-exposure heat treatment with two main objectives: **(i)** to evaluate whether the degradation of K_R could be restored by post-exposure heat treatments, and **(ii)** to evaluate whether the heat treatment aids in reducing the secondary cracking prevalence. The study will, therefore, indirectly evaluate the role of hydrogen in the degradation of the fracture toughness and surface integrity of the material.

2 Materials and Methods

2.1 Materials

The material under consideration in the current investigation is 3.2mm thick sheets of wrought aluminium alloy 2024-T3, with the chemical composition summarised in Table 1. Rectangular specimen blanks – with approximate dimensions of 60mm (W_T) x 57.5mm (L) x 3.2mm (B) – were sectioned from the AA2024-T3 sheet material, from which compact tension (C(T)) fracture toughness specimens were produced. The C(T) specimens were machined in accordance to the ASTM E561 [13] standard, with a notch configuration orientated in the L-T direction (refer to Fig 1.a). The envelope of the crack starter notch is depicted in Fig. 1, and comprised of a typical straight-through notch, terminating in a narrow-type notch* (refer to Fig. 1.b). The specimens were subjected to cyclic loading in order to

* Terminology used in reference to the ASTM E1820-23a Standard (reference [14])

produce a fatigue pre-crack that extends at least 1.3mm from the starter-notch configuration. Ultimately, thirteen C(T)(L-R) specimens were produced with an approximate C(T) specimen width (W) of 48mm, length (L) of 57.5mm and a thickness (B) of 3.20mm. The initial crack length (a_0) of all specimens fell within the 0.35 – 0.55W range prescribed in the ASTM E561 Standard. Finally, tensile test specimens (with the dimensions shown in Fig. 2) were also machined from the aluminium sheet, with the main goal of establishing the yield strength for the various material conditions considered in the current investigation, to facilitate the determination of the plastic zone dimensions.

Table 1 Chemical composition of the material studied [15] compared to the AA2024 specification in the ASTM B209/B209M Standard [16]

		Si	Fe	Cu	Mn	Mg	Cr	Zn	Ti	Al
Aluminium alloy 2024 (ASTM B209/B209M)	**max**	0.50	0.50	4.9	0.9	1.8	0.1	0.25	0.15	rem.
	min	-	-	3.8	0.3	1.2	-	-	-	
Chemical analysis results		0.50	0.50	4.35	0.64	1.50	0.10	0.25	0.15	rem.

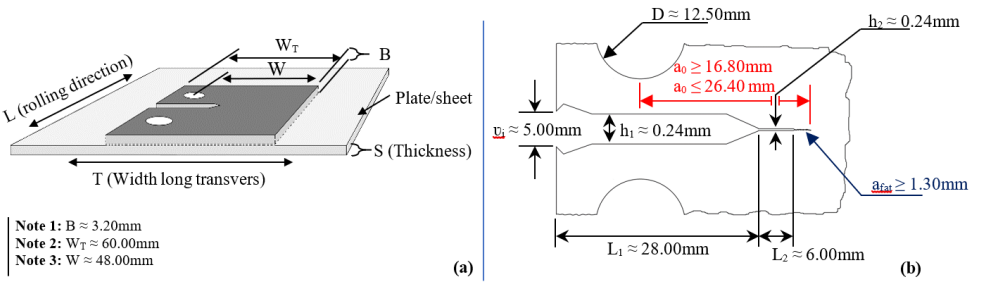

Fig. 1 Schematic representation of **(a)** the L-T orientation of the compact tension specimen as compared to the rolling direction and specimen dimensions, **(b)** the specimen notch/pre-crack configuration.

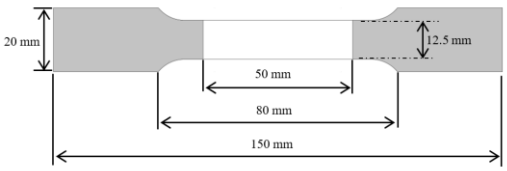

Fig. 2 Schematic representation of tensile specimen with the relevant dimensions (thickness of 3.2mm).

2.2 Methods

It has earlier been shown that a part of the tensile material property degradation observed in AA2024 – due to the corrosive exposure of the alloy to an EXCO-solution – may be recovered via post-exposure heat treatments [10]. This has been attributed to the desorption of hydrogen from the alloy, and serves as a method to establish to what extent diffusible hydrogen contributes to the material property degradation. The current investigation follows a similar methodology, but with specific methods introduced to evaluate hydrogen embrittlement effects on crack extension resistance. Specifically, the aim the work is to establish whether corrosion-induced hydrogen embrittlement affects the slow strain rate,

crack extension resistance behaviour of AA2024-T3, and the formation of the secondary cracks. The experimental procedure can be subdivided into two main categories, namely baseline tests and EXCO-exposed tests. Regarding the first category, the K_R tests aim to establish the baseline crack extension resistance behaviour of the AA2024-T3 material at slow strain rates, as well as the effect of the heat treatment on these properties prior to any corrosive exposure. As such, the baseline tests can be further subdivided into two subsets of tests: **(i)** baseline K_R tests performed on the as-produced AA2024-T3 material (hereafter designated by AA2024-T3 BL tests), and **(ii)** K_R tests performed on heat treated specimens. The heat treatment comprised of a two-hour solution heat treatment at a temperature of 493ºC, followed by a water quench and an artificial ageing heat treatment at 191ºC for 9 hours. The aim of the heat treatment is to simulate a T62 heat treatment according to the ASTM B918/B918M Standard [17] These specimens will therefore be designated by AA2024-T62 BL. Regarding the EXCO-exposed (category two) tests, the K_R tests may once again be subdivided into non-heat treated and exposed (hereafter designated by AA2024-T3 EE) and post-exposure heat treated (AA2024 (EE) -T62) specimens. In both cases, the as-produced C(T) specimens were exposed to an EXCO-solution (refer to section 2.2.1) for two hours prior to K_R testing. However, whereas the AA2024-T3 EE specimens were exposed to slow strain rate K_R testing directly after exposure, the AA2024 (EE)-T62 specimens were first exposed to the T62 heat treatment before slow strain rate K_R testing. Fig. 3 summarises the experimental procedures.

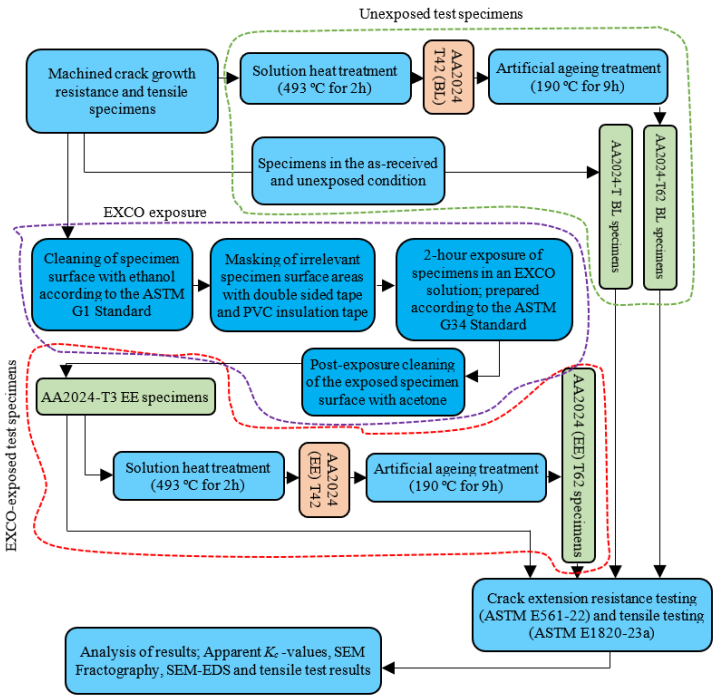

Fig. 3 Schematic diagram illustrating the experimental procedures used in this study

2.2.1 Preparation of the EXCO-solution and K_R specimen exposure

The EXCO-solution was prepared in accordance to the ASTM G34 Standard [18] by dissolving 234 g of sodium chloride and 50 g of potassium nitrate to 700 ml of distilled water. The mixture was stirred vigorously until the reagents were dissolved/saturated before adding

6.3 ml of concentrated (70 wt%) nitric acid. Thereafter, the solution was diluted to 1 litre using distilled water, and stirred for another two minutes before transferring to a sealed glass container.

Prior to the exposure of the selected K_R specimens to EXCO-solution, the specimens were cleaned in ethanol for 3 minutes. Most of the external surface of the specimens were shielded off with PVC tape in order to reduce the exposure area to a 12 mm wide region near the notch/ pre-crack configuration. The specimens were then exposed to 200 ml of the EXCO-solution at 25 ºC, complying to the 10-30 mL/cm^2 range of volume-to-metal surface area ratio as prescribed by the ASTM G34 Standard. Deviating from the standard, the specimens were only exposed for 2 hours, in order to simulate the early stages of atmospheric corrosion. Thereafter, they were removed from the solution and washed in ethanol before removing the shielding. After the removal of the shielding, another 5 min acetone wash was performed. The AA2024-T3 EE specimens were subjected the slow strain rate K_R testing immediately after exposure, whereas the AA2024 (EE) T62 specimens were thereafter subjected to solution and subsequent ageing heat treatments.

2.2.2 Slow strain rate K_R test procedure

The slow strain rate K_R tests were performed on an MTS Criterion 45 Static Test system. The MTS Elite Test Suite software was programmed to load the specimen in accordance to the unloading compliance method as described in the ASTM E561 Standard [13], and provided the relevant load/crack-mouth-opening (CMOD) data as an output for the individual K_R tests. The output data was then processed using the equations derived for C(T) specimens, as prescribed in the ASTM E561 Standard [13]. Deviating from the standard, the software was set to strain the K_R specimen at a fairly slow cross-head displacement rate of $5x10^{-4}$ mm/s, with the test set to terminate once a CMOD of 3 mm is achieved. Due to the slow displacement rate required for the evaluation of hydrogen embrittlement effects, the rate of change in stress intensity for the initial portion of the loading curve did not fall in the specified 0.55-2.75 MPa·√m·s^{-1} range. Therefore, the fracture toughness values determined via the current method will not yield ASTM E561 compliant K_C fracture toughness values, but rather serve as a comparative tool for evaluating the effect of both the corrosive exposure and the heat treatments on the non-plane strain fracture toughness at slow strain rates. The relevant specimen dimensions were measured both prior to and after K_R testing. For each exposure condition, at least a duplicate of tests was conducted.

2.2.3 SEM microscopy, fractography and EDS analysis

Scanning electron microscopy (SEM) was performed using a Zeiss 540 Cross-beam FEG SEM at an excitation voltage of 20 kV. Prior to the breaking open of the K_R specimens, SEM microscopy was performed on exposed surfaces of the EXCO-exposed specimens, with the aim of evaluating the extent of secondary cracking observed within the plastic zone. Energy dispersive X-ray spectroscopy mapping was performed on the exposed specimen surfaces ahead of the plastic zone. Thereafter, the specimens were cracked open, and the fracture surfaces of specimens from all exposure conditions were evaluated after washing in alcohol to remove any dust particles.

2.2.4 Tensile testing:

The tensile specimens were subjected to similar exposure conditions as described for the K_R specimens. Regarding the specimens that were exposed to the EXCO-solution, the PVC

shielding of majority of the specimen surface prior to the EXCO exposure was done in such a manner as to ensure that the corrosion exposure was localised to the 50 mm gauge length. The specimens were tested using an MTS Criterion 45 test system operated with MTS Test Suite software at a displacement rate of 5 x 10^{-3} mm·s^{-1}. Two specimens were tested for each material condition.

3 Results and discussion

3.1 Tensile test results:

In order to establish the crack extension resistance (K_R) behaviour, the yield strength of the material needs to be established first. This is due to the use of the yield strength in the calculation of the plastic zone size and the K_R curve according to the following equations:

$$K_R = K_{(a_e)} = f(P, W, B, a_e) \quad (1)$$

with: $$a_e = a_p + r_y \quad (2)$$

and $$r_y = \frac{1}{2\pi}\left(\frac{K_{(a_p)}}{\sigma_{YS}}\right)^2 \quad (3)$$

According to the equations, the K_R value for the C(T) specimen geometry is a function of the applied load (P), specimen width (W) and thickness (B), and effective crack length (a_e) (equation 1). The effective crack size is calculated as the sum of the physical crack size (a_p) and the plastic zone size (r_y) (refer to equation 2), with r_y a function of the applied stress intensity (at the physical crack size, $K_{(ap)}$) and the yield strength of the material (equation 3). It is clear that the heat treatment and exposure conditions may alter the yield strength of the material. As such, tensile tests were performed in order to establish the yield strength of the various material conditions, as summarised in Table 2.

Table 2 Summary of the tensile mechanical property results of the aluminium alloy 2024 according to material condition.

	$R_{p,0.2}$ (MPa)	R_{UTS} (MPa)	A_{50} (%)	U_T (MJ/m^3)
AA2024 T3-BL	336±1	481±1	16.8±1.2	68.8
AA2024 T3-EE	321±3	454±5	14.2±0.26	55.1
AA2024 T64 BL	349±2	457±1	10.8±0.6	43.8
AA2024 (EE) T64	349±4	443±2	10.2±1.2	40.6

Regarding the T3 condition, a decrease of approximately 15 MPa is observed in the yield strength ($R_{p,0.2}$) after the short-term exposure of the aluminium alloy to the EXCO solution. Similarly, the tensile strength (R_{UTS}) and elongation to fracture (A_{50}) also decreased by approximately 27 MPa and 2.6 % respectively. The solution and ageing heat treatment increased the $R_{p,0.2}$ by approximately 13 MPa, whilst lowering the R_{UTS} by approximately 24 MPa. Additionally, a degradation was also observed in A_{50} of approximately 6 %. Short-term EXCO exposure prior to the heat treatment revealed little to no effect on $R_{p,0.2}$ and A_{50} when compared to the baseline heat treated material. However, the tensile strength was degraded by a further 14 MPa (-38MPa when compared to the AA2024 T3-BL material).

In Table 2, the term U_T has been used as an indicator of the material toughness during uniaxial tensile loading conditions. It is the approximate area underneath the tensile stress-strain curve, calculated using equation 4:

$$U_T = \frac{(R_{p,0.2}+R_{UTS})A_{50}}{2} \quad (4)$$

It is clear from Table 2 that the tensile toughness decreases in the listed order. Comparing the baseline T3 and heat-treated material, the U_T - results imply that the toughness has been degraded by the heat treatment. Additionally, the EXCO exposure also altered the toughness properties, with a smaller effect seen after the heat treatment. The K_c- values can be expected to show a similar trend to that observed for U_T.

3.2 Crack extension resistance testing

3.2.1 The effect of the heat treatment on the crack extension resistance behaviour of the AA2024

The baseline slow strain rate K_R results are summarised in Fig. 4. Regarding the as-produced samples (Fig. 4.a), an effective critical crack extension resistance value ($K_{c,eff}$) of 93.0±1.1 MPa√m was established when using the unloading compliance method. The results compare well with the measured K_c results of Pretorius et. al. [11], with a reported fracture toughness of 91±2 MPa√m. The $K_{c,eff}$ values reported in the current work are not claimed to reflect K_c values that are fully compliant with the ASTM E561Standard, due to the slow strain rate requirement of the hydrogen embrittlement tests. Additionally, the validity of the calculated K_R value assumes that the uncracked ligament of material remains predominantly elastic [13]. This condition is met when equation 5 is upheld:

$$r_y \leq \frac{1}{8}\left(W - a_p\right) \quad (5)$$

with r_y, W, and a_p having the same meanings as stated before.

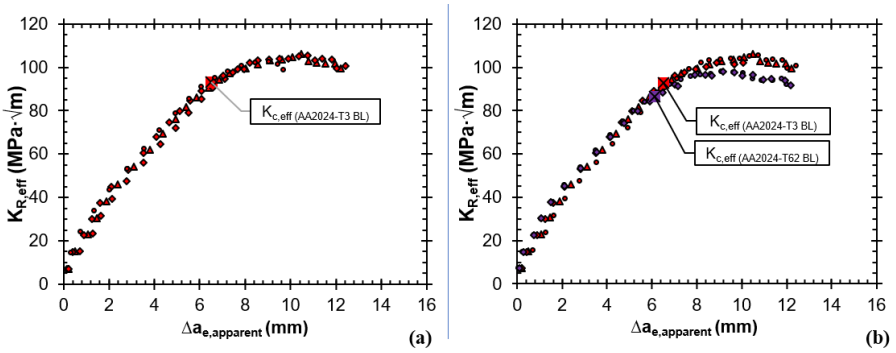

Fig. 4 K_R curves showing the effective resistance to crack extension ($K_{R\_effective}$) as a function of the apparent effective crack extension ($\Delta a_{e,apparent}$) for **(a)** the as-produced AA2024-T3 specimens (red), and **(b)** the heat treated AA2024-T62 specimens (purple) as compared to the AA2024-T3

However, it was found that the validity requirement of equation 5 is only upheld for K_R values up to 55±2MPa√m for the unexposed material. Thereafter, the size of the calculated plastic zone (r_y) exceeds 1/8th of the remaining ligament of material (W-a_p). The result is that the K_c value determined at the maximum applied load did not fall within the validity requirements of the ASTM E561 Standard and, as such, does not yield valid K_C fracture toughness values for the material. Therefore, the K_R and K_c values reported in this work will

be referred to rather as $K_{R,eff}$ and $K_{c,eff}$ respectively. Nevertheless, it is proposed that the method may still prove useful for comparative purposes when evaluating the effect of hydrogen embrittlement. This appears to be substantiated by the relatively low degree in scatter (±1 MPa√m) observed in the AA2024-T3 BL test results, and the good comparability with the results of Pretorius et. al. [11].

The heat treatment resulted in a decrease in the $K_{C,eff}$ to approximately 86.7±0.7MPa√m. This may be explained by considering the tensile test results discussed in section 3.1. It has been established that the heat treatment slightly increases the yield strength, and decreases the tensile toughness. According to equation 3, a larger yield strength will reduce plastic zone size. This implies that, although a larger load may be required for crack extension, a smaller volume of material will absorb the applied energy through plastic response. Additionally, the U_T results indicate that the plastically strained material would be able to absorb less of the applied energy for the heat-treated case. As such, the applied energy acts on a smaller volume of material that has a reduced ability to absorb the energy, resulting in a lower fracture toughness.

3.2.2 The effect of the exposure and post-exposure heat treatments crack extension resistance behaviour of the AA2024-T3

The effect of the EXCO exposure on the $K_{R,eff}$ curves can be seen in Fig. 5. The $K_{R,eff}$ curves in Fig. 5.a compares the results for the AA2024-T3 BL material (red plot) to the AA2024-T3 EE material. A drop in the $K_{c,eff}$ value from 93.0±1.1MPa√m to 87.3±0.7MPa√m is observed. As discussed at a later stage, this equates to a loss in fracture toughness of approximately 6.1%. However, it is worth noting that a larger loss will be observed if one assumes that the yield remained unchanged as a result of the EXCO exposure. With that assumption, the K_R results would reveal a reduction in the fracture toughness to 83.9±0.4MPa√m, a 9.8% reduction in the effective fracture toughness, which shows good correlation with the 11.2±0.1% earlier reported by Pretorius et.al. [11]. The observed reduction in the yield strength will however be incorporated for the current investigation.

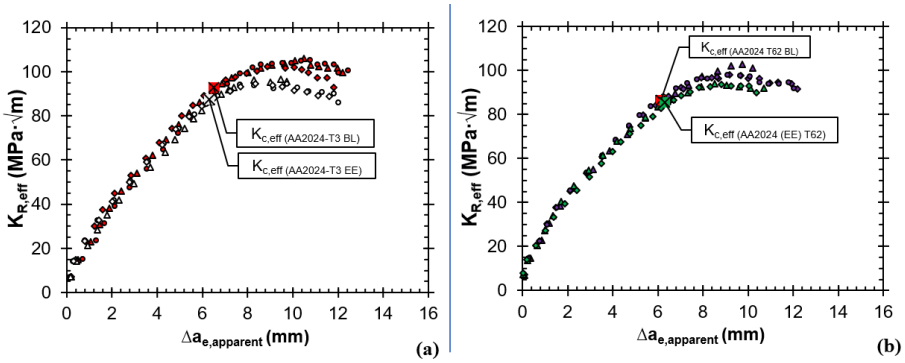

Fig. 5 K_R curves comparing the effective resistance to crack extension ($K_{R\_effective}$) as a function of the apparent effective crack extension ($\Delta a_{e,apparent}$) of **(a)** the as-produced (AA2024-T3 BL) specimens (red) and the EXCO exposed AA2024-T3 (EE) specimens (white), and **(b)** the unexposed (purple) and EXCO exposed (green) heat treated specimens..

The K_R curves in Fig. 5.b compares the results for the AA2024-T64 BL material (purple plot) to that of the AA2024 (EE) T64 material. Fairly similar crack extension behaviours are noted for the two material conditions, with the prior EXCO exposed material showing a slight

decrease in the $K_{c,eff}$ to 85.4±0.1MPa√m. This indicates a degradation of only 1.4% when compared to the AA2024-T64 BL material.

3.3 Scanning electron microscopy

3.3.1 Fractography results on the primary crack front

The general fracture morphologies observed on the primary crack front during the slow strain rate K_R testing of the aluminium alloy 2024-T3 has been discussed in the work by Pretorius et.al. [11]. Similar fracture morphologies are observed in the current work, with Fig 6. showing the features common to all material conditions. All exposure conditions comprised of a fatigue pre-cracked region (labelled (i), SEI in Fig. 6.c), a triangular region of (ductile) stable crack extension ((ii), SEI in Fig 6.d) orientated perpendicular to the loading axis, and a 45º shear overload (unstable) fracture region (labelled (iii), SEI in Fig. 6.e).

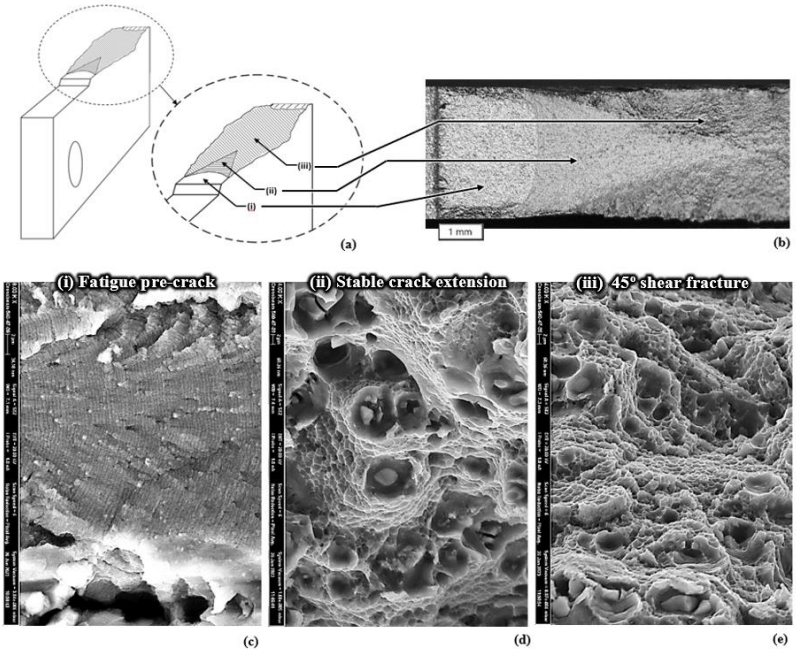

Fig. 6 (a) Illustration showing the general fracture morphologies that were observable in all test specimens after testing, with **(b)** an overview stereo-fractograph (8X nominal), and **(c)** through **(e)** secondary electron images (SEIs) of the fracture morphologies (4000X nominal)

Of importance in the current investigation, is the fracture morphology associated with the the primary crack close to the external surface and within the stable crack extension region. Fig 7. and Fig.8 summarise the fractography results at these locations for the unexposed and EXCO exposed specimens. For both unexposed material conditions, a ductile (dimpled) fracture morphology was observed near the external surfaces (refer to Fig 8). After exposure to the EXCO solution, however, a transition is seen towards intergranular cracking, which is observed near the external (exposed) surfaces of AA2024-T3 (refer to Fig. 8.a). The intergranular cracking was also observed to remain after the post-exposure heat treatment (refer to Fig. 8.b).

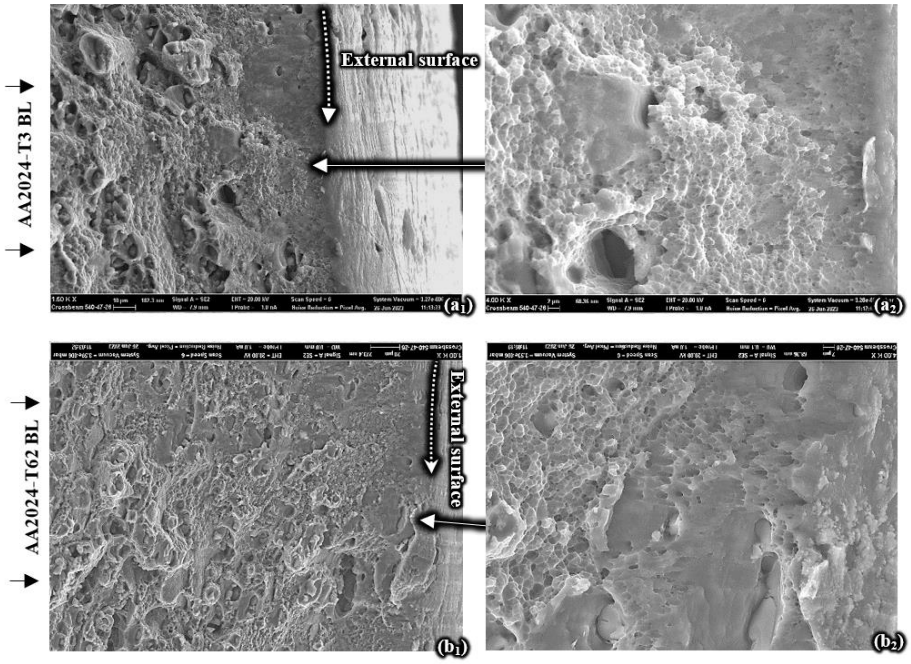

Fig 7. Fracture morphologies observed near the external surfaces of the **(a)** AA2024-T3 BL and **(b)** the AA2024-T62 BL specimens. **Nominal magnifications: (a_1)** 1500X, **(b_1)** 1000X, and **(a_2)** and **(b_2)** 4000X

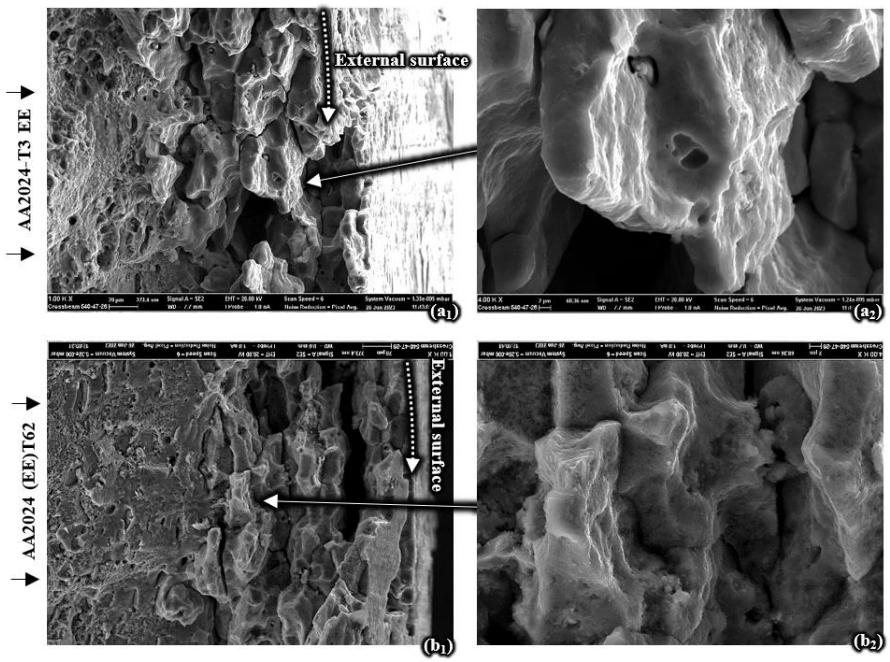

Fig 8. Fracture morphologies observed near the external (exposed) surfaces of the **(a)** AA2024-T3 EE and **(b)** the AA2024 (EE) T62 specimens. **Nominal magnifications: (a_1)** and **(b_1)** 1000X, and **(a_2)** and **(b_2)** 4000X

3.3.2 Secondary cracking observed on the EXCO-exposed specimens

The secondary cracking observed on the AA2024-T3 C(T) specimen after exposure to an EXCO solution has been documented in the work by Pretorius et.al [11]. Similar cracking behaviour was observed in the current study for the AA2024-T3 EE specimens, and was found to persist after the post-exposure heat treatment (yellow arrowed in in Fig. 9.a). The intergranular nature of these cracks can be observed in the secondary electron images (SEIs) in Fig. 9.b. At locations outside of the plastic zone – produced during K_R testing – these secondary cracks are no longer visible (Fig. 9.c). However, at some locations, apparent grain-boundary attack (white arrowed) was observed at 1500X nominal magnifications. Preliminary energy dispersive X-Ray spectroscopy (EDS) mapping also revealed an increase in the detection of magnesium within the grain-boundaries (refer to the Mg-$K_{\alpha 1\_2}$ map in Fig. 9.d), indicating enrichment in magnesium within the grain-boundaries. Finally, some micro-scale pitting (white arrowed) was also observed. This type of corrosion attack appears to be associated with the copper-rich constituent particles, and is likely a result of trenching due to the well-defined micro-galvanic mechanism of corrosion associated with aluminium constituent particles.

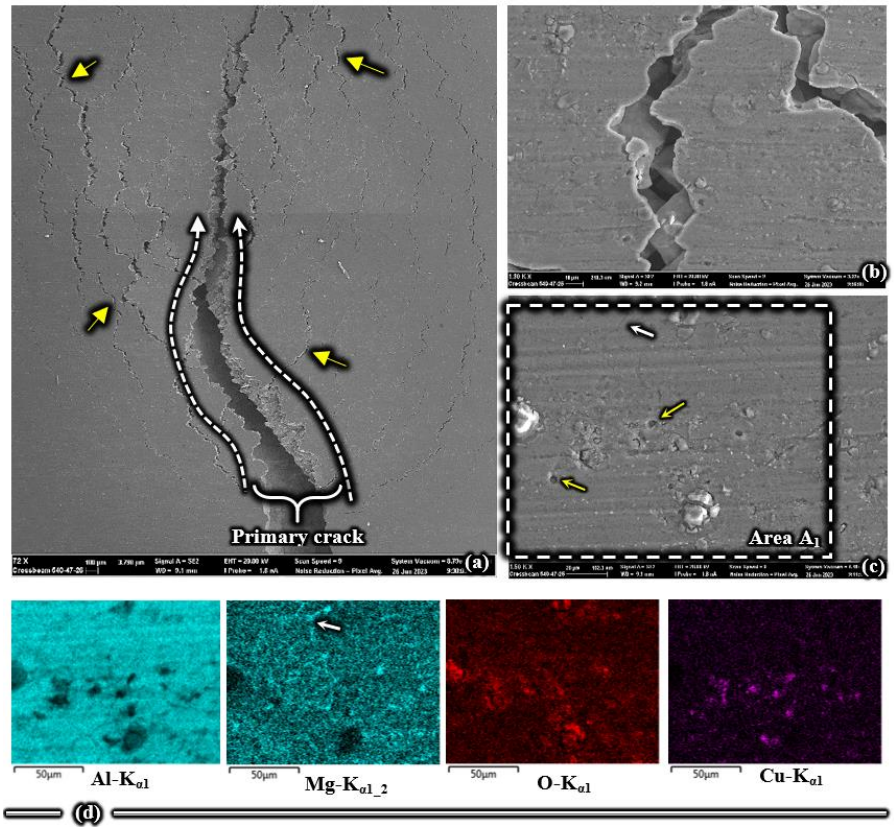

Fig. 9 SIEs and EDS maps showing the typical morphology of the exposed surface of the AA2024 (EE) T62 specimens after K_R testing; (a) near the primary crack (76X nominal), (b) higher magnification (1300X nominal) SIE of secondary cracks, (c) outside the plastic zone (1500X nominal), and (d) the SEM EDS map results for area A_1 in (c).

4 Summary of results

Fig. 10. summarises the fractional loss in toughness due to the treatment of the material as compared to the unexposed 3.2mm thick AA2024-T3 alloy. The fractional loss (f_{loss}) was determined using equation 6, with the fraction of original toughness (f_{KC}) given by equation 7:

$$f_{loss} = \frac{K_{C,i} - K_{C,AA2024-T3\ BL}}{K_{C,AA2024-T3\ BL}} \quad (6)$$

$$f_{KC} = \frac{K_{C,i}}{K_{C,AA2024-T3\ BL}} \quad (7)$$

with $K_{c,i}$ referring to the $K_{c,eff}$ value for the relevant exposure condition, and $K_{c,AA2024\text{-}T3Bl}$ the baseline K_c values of the unexposed material. The heat treatment resulted in a decrease in the fracture properties of ≈ 6.8±0.7% (refer to AA2024-T64). The decrease in the fracture toughness is attributed to microstructural differences due to the heat treatment, as reflected by the increased yield strength (reducing the plastic zone size) and the reduced uniaxial toughness (U_T) established during tensile testing. Short-term (2 hour) exposure of the AA2024-T3 alloy to an EXCO solution resulted in a reduction in K_c toughness of ≈ 6.2±0.7%. This is less than the 11.2% earlier reported by Pretorius et.al. [11]. However, if the yield stress is assumed to remain unchanged (i.e. assuming the 336 MPa yield stress of the AA2024-T3 BL material), a degradation closer to that of Pretorius et.al. would be observed (≈9.8±0.4%). It could be argued that the corrosion-induced hydrogen embrittlement caused the observed reduction in the yield strength, and that the use of the reduced yield strength values in the $K_{c,eff}$ calculations reduces the fracture toughness hydrogen embrittlement effect. This appears to be supported by the tensile test results of the post-exposure heat treated specimens, in which a similar yield strength was observed between the AA2024 (EE) T62 and AA2024-T62 BL specimens, thereby indicating that the yield strength was restored due to hydrogen desorption. Nevertheless, the yield strength established during tensile testing is used in the calculation of $K_{R,eff}$ in the current investigation. This results in a similar trend in the $K_{c,eff}$ and U_T values.

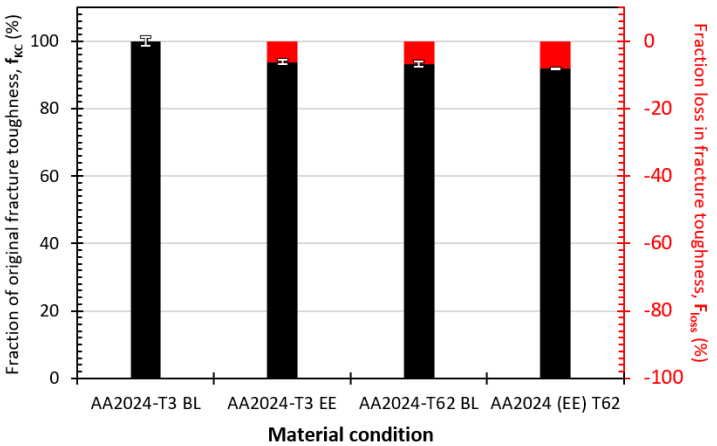

Fig. 10 Comparison of the $K_{c,eff}$ test results according to the fraction of original toughness and fractional loss in toughness

Post-exposure heat treatment of the aluminium alloy 2024-T3 revealed a degradation in $K_{c,eff}$ of 8.1±0.1% when compared to the AA2024-T3 BL specimens (see bar chart for AA2024 (EE) T62 in Fig. 10). However, when compared to the heat treated baseline specimens (AA2024-T62 BL), a further degradation in $K_{c,eff}$ of only 1.4±0.1% (8.1 % vs 6.7 % average) is observed. This observation implies that the heat treatment restored most of the degraded fracture toughness resulting from the short-term EXCO exposure. The small change in the $K_{c,eff}$ values may be attributed to either scatter in the results, or to the secondary surface cracking observed in the plastic zone during scanning electron microscopy. It was shown that the intergranular secondary cracking (ISC) – originally observed on the AA2024-T3 EE specimens – persisted after the post-exposure heat treatment. This may also explain the reduction in the tensile strength observed during tensile testing for the exposed samples.

The scanning electron microscopy results also revealed indications of localised intergranular attack and micro-scaled trenching on the exposed surfaces of the AA2024 (EE) T62 material at locations outside of the plastic zone. Magnesium enrichment was detected within the former using energy dispersive X-ray spectroscopy (EDS). The pitting was found to be associated with copper rich particles/precipitates. The formation of aluminium hydrides as a possible cause of the ISCs need to be investigated. Further SEM and XRD studies will be performed in order to investigate this aspect in more detail.

5 Conclusions

1. A significant degradation was observed in the slow strain-rate $K_{c,eff}$ after short-term (2 hour) exposure of the AA2024-T3 K_R specimens to the EXCO-solution.

2. Post-exposure heat-treatments restored the majority of the fracture toughness reduction (slow strain-rate $K_{C,eff}$), indicating that the degradation in the crack extension resistance behaviour was caused by corrosion-induced (diffusible) hydrogen embrittlement

3. The secondary surface cracks that formed in an intergranular fashion in the plastic zone of aluminium alloy 2024-T3 K_R specimens after short term exposure to an EXCO solution, were found to persist after performing solution and ageing heat treatments

6 Further work

Further SEM studies are proposed in order to evaluate whether any intergranular constituents are detectable prior to straining; including but not limited to intergranular hydride formation. In addition, measurement of diffusible hydrogen content for the conditions investigated should be performed.

The financial funding from the Light Metals Development Network (LMDN) forming part of DSI is greatly acknowledged. The team of Prof. Nikos Alexopoulos from the University of the Aegean, Greece, is acknowledged with great thanks for the provision of the AA2024-T3 material.

References

1. R. Revie, *Uhlig's Corrosion Handbook (3rd Edition)*, John Wiley & Sons, 762-740 (2011).

2. G. Svenningsen, J.E. Lein, A. Bjorgum, J.H Nordlien, Y.D. Yu, K. Nisancioglu, Corros. Sci. **48** 258-272 (2006)
3. G. Svenningsen, M.H. Larsen, J.C. Walmsley, J.H. Nordlien, K. Niscancioglu, Corros. Sci. **48,** 3969-3987 (2006)
4. L. Lacroix, L. Ressier, C. Blanc, G. Mankowski, J. Electrochem. Soc. **155,** C131-C137 (2008)
5. C. Blanc, A. Freulon, M.C. Lafont, Y. Kihn, G. Mankowski, Corros. Sci. **48,** 3838-3851 (2016)
6. P. Campestrini, E.P. van Westing, H.W. van Rooijen, J.H. de Wit, Corros. Sci. **48,** 1853-1861 (2000)
7. G. Guo, Y. Li, H., Li, X. Peng, J. Li, G. Xu, Mat. and Des. **223** 1-14 (2022)
8. C. Lou, X. Zhou, G.E. Thompson, A.E. Hughes, Corros. Sci. **61**, 35-44 (2012)
9. X. Zhang, Y. Jiao, Y.Yu, B. Liu, T. Hashimoto, H. Liu, Z. Dong, Corros. Sci. **155**, 1-12 (2019)
10. P.V. Petroyiannis, Al.Th. Kermanidis, P. Papanikos, Sp.G. Pantelakis, Theoretical and Applied Fracture Mechanics **41**, 173-183 (2004)
11. C.C. Pretorius, R.J. Mostert, S. Ramjee, SAIMM **121**, 151-158 (2021)
12. C. Larignon, J. Alexis, E. Andrieu, L. Lacroix, G. Odemer, C. Blanc, Electrochimica Acta **110**, 484-490 (2013)
13. ASTM E561-22, Standard method for K_R curve determination, ASTM International (2022)
14. ASTM E1820-18, Standard test method for measurement of fracture toughness, ASTM International (2018)
15. C-M. Charalampidou, C.C.E. Pretorius, R.J. Mostert, N.D. Alexopolous, Corrosion 77, 1029-1040, (2021)
16. ASTM B209/B209M-21a, Standard specification for aluminium and aluminium-alloy sheet and plate, ASTM International (2021)
17. ASTM B918/B918M-20a, Standard practice for heat treatment of wrought aluminium alloys, ASTM International (2020)
18. ASTM G34-01, Standard test method for Exfoliation Corrosion Susceptibility in 2XXX and 7XXX series aluminium alloys (EXCO test), ASTM International (2018)
19. M.J. Haynes, R.P. Gangloff, JTEVA **25**, 82-98 (1997)